DOI: 10.24996/ijs.2026.67.7.37

ISSN: 0067-

Determining The Locations of Calcium Deposits in Iraq Using Image Processing and Satellite Images

Khaleel Ibrahim Abood*1, Faleh Hassan Mahmood[1], Susan A. Mohammed Taqi[2]

[1]Remote Sensing Unite, College of Science, University of Baghdad, Iraq, [3] Ministry of Higher Education and [2]Scientific Research, Scholarship and Culture Relations Department, Iraq

Received: 15/12/2024 Accepted: 30/ 6 /2025 Published: 30/7/2026

Abstract

This study employs a photometric technique to investigate the intensity of color gradients within image pixels. The MATLAB software was developed to evaluate laser spots by computing the average wavelength from pixel values in pictures, resulting in an overall error rate ranging from 1% to 10%, depending on the exact laser wavelength examined. The program executes pixel-wise wavelength estimation by transforming color intensity gradients into wavelength values and then conducts statistical analysis of several laser spots to ensure precision. These techniques facilitated the identification of spectral lines corresponding to the mean wavelength of each laser source. The methodology was initially validated by measuring the monochromatic wavelengths of the laser beams. The MATLAB program for image processing effectively identified laser wavelengths at 325, 473, 477, 535, 603, and 785 nm, producing outstanding results with negligible error rates. This study employs advanced methods to identify specific wavelengths associated with naturally occurring elements in soil or land. The methodology emphasizes the distinct wavelength properties of each element, incorporating Google Earth Maps for spatial analysis and MATLAB for data processing and visualization. The land area was progressively enlarged to identify the calcium deposit fields until it reached an elevation of approximately 700 m above sea level, with an image width of only 200 m, resulting in each pixel representing only 24 cm. A calcium deposit field in the Anbar region was selected as the specimen for the unexamined calcium field. The analysis identified calcium deposit locations on the map, demonstrating that Iraq possesses abundant calcium resources, particularly in the western and southwestern regions. The findings of this study enable companies to precisely identify calcium-rich areas, thereby minimizing extensive fieldwork, conserving financial resources, and decreasing the time required to locate the sources of this element and its compounds.

Keywords: Soil Elements, satellite images, calcium deposits, Image processing.

تحديد مواقع رواسب الكالسيوم في العراق باستخدام معالجة الصور وصور الأقمار الصناعية

خليل إبراهيم عبود*1، فالح حسن محمود[1]، سوزان علي محمد تقي[2]

[1] وحدة الاستشعار عن بعد ، كلية العلوم، جامعة بغداد، العراق

[2] وزارة التعليم العالي والبحث العلمي، دائرة البعثات والعلاقات الثقافية، العراق

*Email: Khaleel.i@sc.uobaghdad.edu.iq

الخلاصة:

تستخدم هذه الدراسة تقنيةً ضوئيةً لفحص شدة تدرجات الألوان في بيكسلات الصورة. طُوِّر برنامج MATLABلتقييم بقع الليزر بحساب متوسط الطول الموجي من بيكسلات الصورة، مما أدى إلى معدل خطأ إجمالي يتراوح بين 1% و10%، ويعتمد ذلك على طول موجة الليزر الدقيق المُفحص. يُجري البرنامج تقديرًا للطول الموجي لكل بيكسل على حدة بتحويل تدرجات شدة اللون إلى قيم طول موجي، ثم يُجري تحليلًا إحصائيًا لعدة بقع ليزر لضمان الدقة. سهّلت هذه التقنيات تحديد الخطوط الطيفية المقابلة لمتوسط طول الموجة لكل مصدر ليزر. تم التحقق من صحة المنهجية في البداية عن طريق قياس الأطوال الموجية أحادية اللون لحزم الليزر. حدد برنامج MATLAB لمعالجة الصور بفعالية أطوال موجية لليزر 325 و473 و477 و535 و603 و785 نانومتر، مما أدى إلى نتائج رائعة بمعدلات خطأ ضئيلة. تستخدم هذه الدراسة أساليب متطورة لتحديد أطوال موجية محددة مرتبطة بالعناصر الموجودة بشكل طبيعي في التربة أو الأرض. تؤكد المنهجية على خصائص الطول الموجي المميزة لكل عنصر، وتدمج خرائط Google Earth للتحليل المكاني و MATLAB لمعالجة البيانات والتصوير. تم توسيع مساحة الأرض تدريجيًا لتحديد حقول رواسب الكالسيوم حتى وصلت إلى ارتفاع يبلغ حوالي 700 متر فوق مستوى سطح البحر، بعرض صورة يبلغ 200 متر فقط، مما أدى إلى تمثيل كل بكسل بـ 24 سم فقط. تم اختيار حقل رواسب الكالسيوم في منطقة الأنبار كعينة لحقل الكالسيوم غير المدروس. حدد التحليل مواقع رواسب الكالسيوم على الخريطة، مما يدل على امتلاك العراق لموارد وفيرة من الكالسيوم، لا سيما في المنطقتين الغربية والجنوبية الغربية. تُمكّن نتائج هذه الدراسة الشركات من تحديد المناطق الغنية بالكالسيوم بدقة، مما يُقلل من الجهد الميداني المكثف، ويُوفر الموارد المالية، ويُقلل الوقت اللازم لتحديد مصادر هذا العنصر ومركباته.

1. Introduction

The Earth's soil consists of diverse elements in the form of salts and oxides[1]. The elements are bound by molecular and atomic bonds, producing various distinct colors. Elements such as copper, iron, gold, and silver exhibit distinct hues that facilitate their identification. Nevertheless, due to their microscopic intermixing, the human eye often cannot distinguish subtle and fine differences between colors. The transition from the use of elements' colors to image processing could be smoother. For example, "Because these elements are often microscopically intermingled, distinguishing their colors with the naked eye is challenging. Image processing technology overcomes this limitation by capturing soil sample images with charged-coupled device (CCD) cameras to capture images of soil samples and employing digital processing techniques to distinguish between these elements [2]. A color image is composed of a two-dimensional array of pixels, where each pixel has an intensity value between 0 and 255 for each of the primary colors that produce all other colors: red, green, and blue. Each of these colors corresponds to a specific wavelength of light. Since the elements have different colors, each element's color ultimately represents a specific wavelength, enabling the identification of different elements based on the colors in the image itself.

Consequently, each image may encompass a range of wavelengths derived from all its pixels, analogous to a spectrum observed in celestial bodies. This general approach enhances the ability to identify and classify soil elements, providing more comprehensive insights into their composition and characteristics. In conjunction with its associated photometry, image processing can be used as a tool for spectral analysis (spectroscopy). Image processing algorithms can replicate spectral analysis by extracting and processing pixel color values that match specific wavelengths of reflected or emitted light. These digital methods facilitate the identification of chemical components or compounds, such as calcium, by comparing the spectral fingerprints (wavelength-dependent reflectance or absorbance patterns) of image regions with established reference spectra.

Any image depicting soils, rocks, or unoccupied terrain has the potential to reveal various indicators about the elements present, as indicated by their colors[3,4]. The method of photometric processing employs several techniques aimed at extracting distinctive features and essential information from digital images and their colors. A CCD camera captures images using an RGB color system, which operates linearly based on the intensity of photons impacting the internal components of the camera. Each photon striking the sensor produces an electrical signal proportional to its energy, enabling the camera to capture fluctuations in light intensity across the entire visible spectrum. This linear response enables the precise quantification of color and brightness in the collected image, making CCD cameras especially suitable for scientific applications that require precise optical measurements, such as remote sensing, spectroscopy, and mineral detection [5,6]. The colors in each pixel of a digital image are dictated by two primary factors: the wavelength of the incoming light and the quantity of input photons, which together establish the photon intensity. The wavelength determines the precise color in the visible spectrum, such as red, green, or blue, while the photon intensity affects the brightness or luminance of that color [7]. Three photon bands exist within the visible spectrum, and the analysis is based on the primary colors: red, green, and blue. Each pixel's color results from a combination of these three colors, with values ranging from zero to 256. Due to the varying probabilities of mixing these colors at different intensities, it is possible to generate up to 16,777,216 unique colors derived from 256 raised to the power of 3 [8]. Ultimately, each pixel in an image is represented by a single color corresponding to the visible wavelength spectrum, which results from mixing three primary colors: red, green, and blue (RGB) [9]. Each color in the visible spectrum is defined by a distinct peak wavelength and an adjacent range of wavelengths that influence its perception. Red typically peaks at around 700 nm, encompassing a broader spectrum from approximately 620 to 750 nm. Likewise, green and blue hues possess distinct peak values and spectrum ranges. This distribution enables nuanced variations in hue and intensity across each color channel (Red, Green, Blue), which are recorded and processed by imaging sensors, such as CCD cameras [10]. In a digital image, each color channel, such as red, green, or blue, is represented by intensity levels ranging from 0 to 255, where 0 indicates the absence of light and 255 indicates the highest intensity that the sensor can perceive. The intensity levels correlate to the quantity of photons detected at specific wavelengths within each color's spectral range [11].

Figure (1) illustrates the three fundamental color bands in the visible spectrum: red, green, and blue, which can combine their intensities to produce all other colors. Some physicists might argue that this is inaccurate, as they believe that the density and intensity of photons do not influence the altered wavelength [12]. However, the reality is that the wavelength does change with variations in photon intensity [13]. This is because the energy of the electric current within the CCD camera's internal components increases as the number of incident photons rises [14].

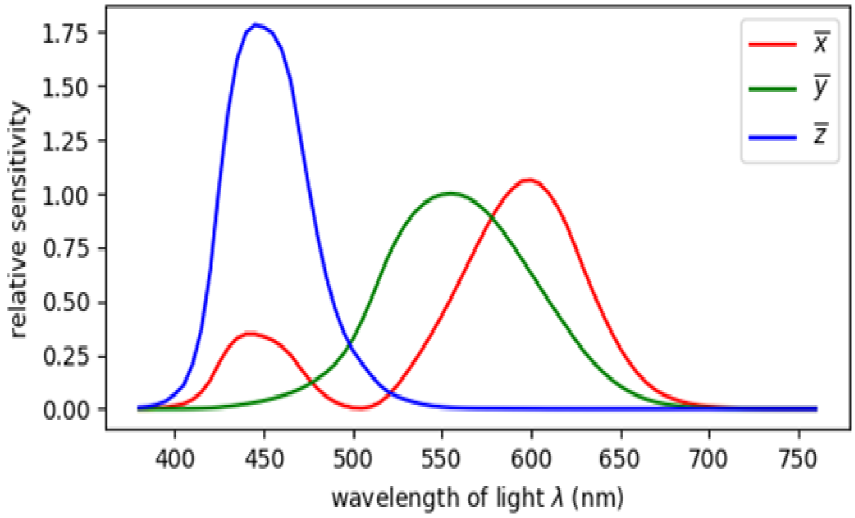

Figure 1: The RGB color model along the visible wavelength spectrum, highlighting the specific ranges for red, green, and blue [15].

Ultimately, each pixel will display a color corresponding to a specific frequency within the visible range [16]. Every element in nature emits multiple strong lines within the human optical range, which eyes perceive as a single color [17]. Consequently, when observing an object composed of mixed elements, it emits various wavelengths, each representing a specific element from each pixel in the image. This results in the target exhibiting distributions of multiple elements across its surface.

This study focused on calcium elements, introducing a novel methodology that utilizes optical range techniques to examine soil components while also emphasizing the importance of validating the program's results. The study's objective is to locate calcium field clusters in Iraq. The results of this study can help companies accurately identify calcium-rich fields, thereby avoiding extensive fieldwork, saving money, and reducing the time required to search for sources of this element and its compounds. Although these studies provide significant insights into mineral identification and mapping, there is a deficiency of targeted studies on calcium localization utilizing image processing approaches. This work presents a novel approach to utilizing optical spectrum analysis for identifying calcium deposits in Iraqi soils. The primary objective is to easily locate high-density calcium zones, thereby reducing the need for extensive field surveys and enhancing the precision and cost-effectiveness of mineral exploration. The subsequent sections of this work are structured as follows: Section 2 reviews the pertinent literature, Section 3 outlines the methodology used in the study, Section 4 analyzes the results and their interpretation, and Section 5 concludes the paper with a summary of the principal findings and prospective research avenues.

2. Literature Review

Several studies have examined the mineral content of the soil, specifically the total presence of iron (Fe) in the Sulaimaniyah Governorate of the Iraqi Kurdistan Region (IKR), which is rich in iron deposits. The spatial quantification and regular monitoring of mineral presence in the soil are crucial in mining areas. A remote sensing technique was employed to forecast soil minerals, specifically iron, in the study area utilizing a multispectral satellite image from the Landsat-7 Enhanced Thematic Mapper Plus (ETM+)[18]. Several other studies in Iraq could benefit from image processing, particularly those related to soil analysis, which aligns with the current study. These investigations focus on analyzing soil samples containing pollutants such as lead and cadmium, which are toxic substances that can infiltrate the human food chain [19].

Babalola et al. presented work on soil image analysis that involved a series of steps to enhance the images. This process included removing non-soil pixels through image segmentation and preparing the images for further analysis. The segmentation was then refined by dividing the images into smaller tiles to isolate soil pixels, followed by high-frequency filtering to improve image quality [20]. Ali Almaliki et al. conducted at a geologically significant and accessible location in Iraq. A digital elevation model (DEM) with a 30-m resolution, obtained from the Shuttle Radar Topography Mission (SRTM), and a geological map were utilized for spatial analysis. These materials facilitated the identification of geographical features and zones of mineral accumulation. Soil samples were collected from various study sites for laboratory analysis. Calcium and magnesium were quantified by classical titration, whereas potassium was assessed using standard analytical techniques [21]. Zeki A. Aljubouri investigated the geochemistry of calcium sulfate rocks within the Fat'ha Formation (Middle Miocene) in northern Iraq, with a particular focus on strontium distribution across various gypsum and anhydrite types. One such study analyzed 90 samples, including anhydrite, massive gypsum, selenite, and fibrous gypsum, from four localities in the Nineveh District[22].

3. Materials and Methodology

The fundamental idea of this research is based on converting the visible color of each pixel in the image to a corresponding wavelength, as each color gradient represents a specific wavelength of light in the visible spectrum. By comparing the wavelength of the pixel color with the specific wavelengths of the element being searched for, using standard references (based on the NIST National Institute of Standards and Technology site for comparison), the presence of that element at a specific location in the image (the map image) can be determined. When the wavelength of the pixel (its color) matches the specific wavelength associated with the element in the standard reference, it indicates the likelihood of that element being present at that location in the image.

During the preliminary phase of the study, the optimal wavelength of monochromatic laser waves was determined using the photometric method, supplemented by image processing techniques. This involved employing spectroscopic techniques, including prisms and diffraction gratings. The initial application concentrated on a green laser with a wavelength of 556 nm. The laser-emitted spotlight was recorded using a conventional mobile phone camera, resulting in a typical photograph, as illustrated in Figure 2. The image was later examined using a custom program to extract the visible spectrum (Figure 3).

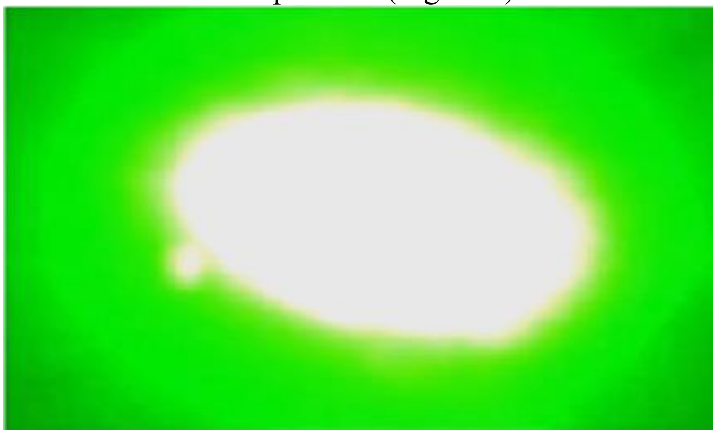

Figure 2: The green laser spot at 556 nm.

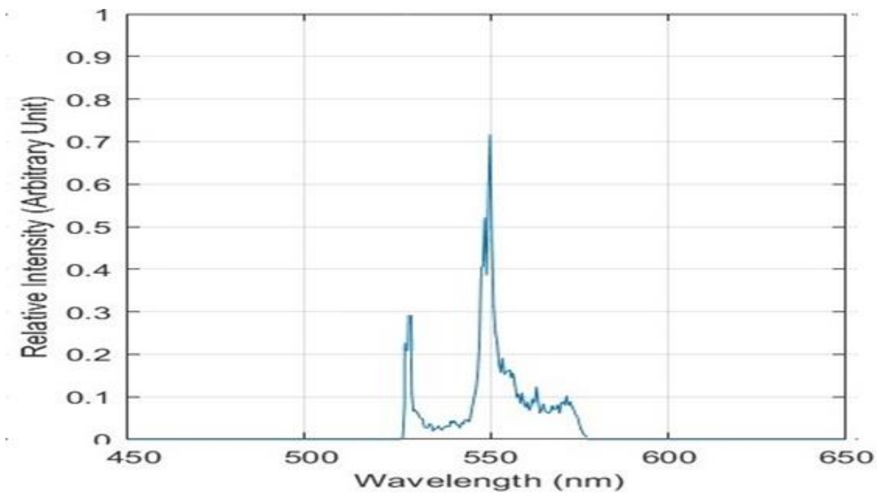

Figure 3: 556 nm laser spectrum extracted using MATLAB.

The MATLAB program analyzed laser spots, yielding an average wavelength of 549 nm and a 1.4% error rate, which is regarded as an excellent outcome. It also presented all spectral lines about this average value. The program underwent testing on multiple laser spots, as illustrated in Figure 4, resulting in a 3.5% error rate for a laser with a wavelength of 473 nm. The findings indicated errors of 1%, 4%, 2.4%, 6%, and 10% for the 477 nm, 603 nm, 535 nm, 785 nm, and 325 nm lasers, respectively.

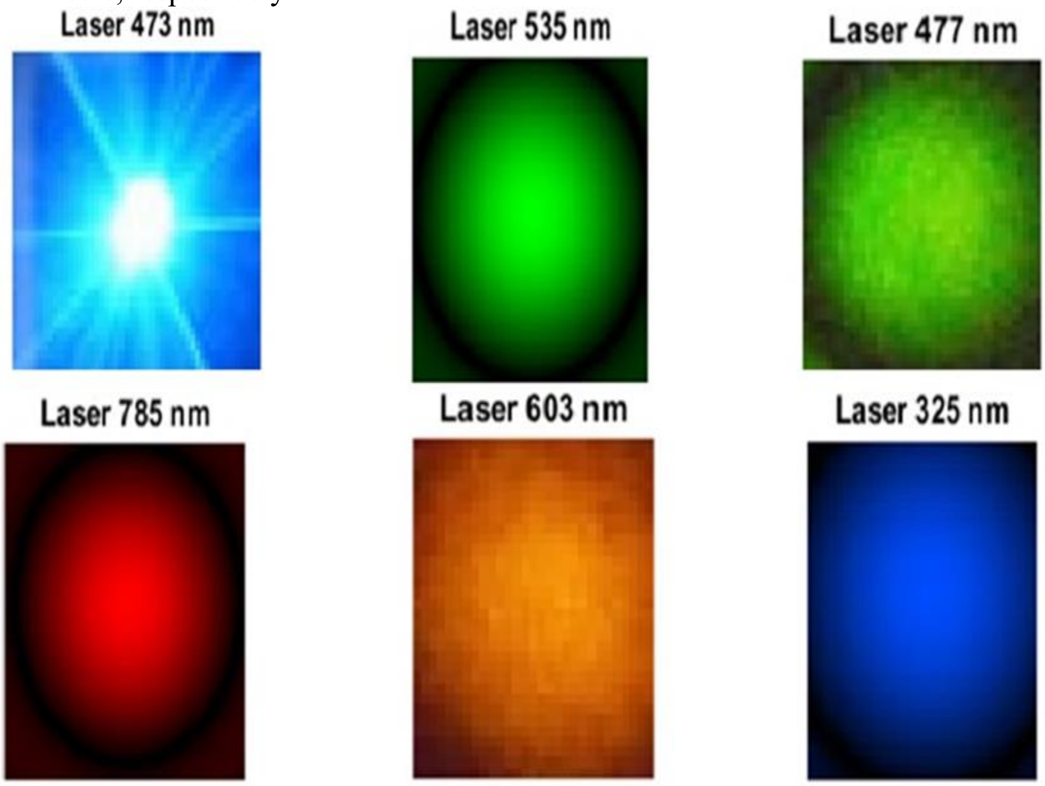

Figure 4: Six laser spots with varying wavelengths [23].

The results summarized in Table 1 indicate the errors in wavelength measurements, highlighting both the potential and the limitations of this method

Table 1: The percent errors by image processing to find the average wavelength of laser spots.

Laser wavelength (nm)	Laser wavelength (nm) after image process	The error
325	357.5	10 %
473	456.4	3.5 %
477	481.7	1 %
535	547.8	2.4 %
603	627.1	4 %
785	737.9	6 %

The laser applications were executed with minimal errors, the maximum being 10% for one laser. Consequently, the program produced outstanding outcomes in the visible spectrum. It can detect elements in diverse natural environments, such as soil and rocks. Each element displays several prominent emission lines in the visible spectrum, correlating with their absorption lines. The observed colors indicate optical reflections rather than direct emission lines.

3. Results and Discussion

3.1. Finding the Elements

Elements display unique colors, including metallic hues, which can be observed in digital images (a program in MATLAB was developed, included entirely in the appendix of the research, for identifying elements. It contains two spectral matrices: one for gold and one for calcium. By replacing the matrix name in the program, the search in the image changes from gold to calcium or vice versa.). The CCD camera captures the intensity of incident photons and converts them into values between 0 and 255 for each color channel of the RGB color space. The color corresponds to the wavelength characteristic of the element, while the photon count indicates the intensity scale. A gold rock will display unique emissions, Figure 5.

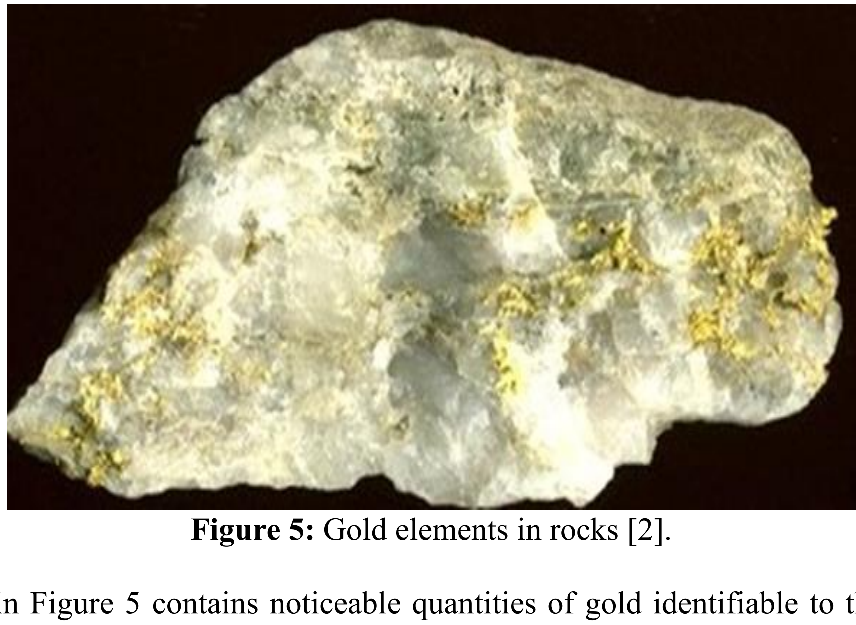

Figure 5: Gold elements in rocks [2].

The rock in Figure 5 contains noticeable quantities of gold identifiable to the naked eye. Nonetheless, the difficulty lies in identifying and evaluating it solely through software employing image-processing methodologies. By implementing intricate procedures, conducting experimental analysis, and applying specific physical relationships for element identification, a methodology was developed for identifying elements in images using the MATLAB program, Figures 6 and 7.

Figure 6: MATLAB program identifies gold element by red color [2].

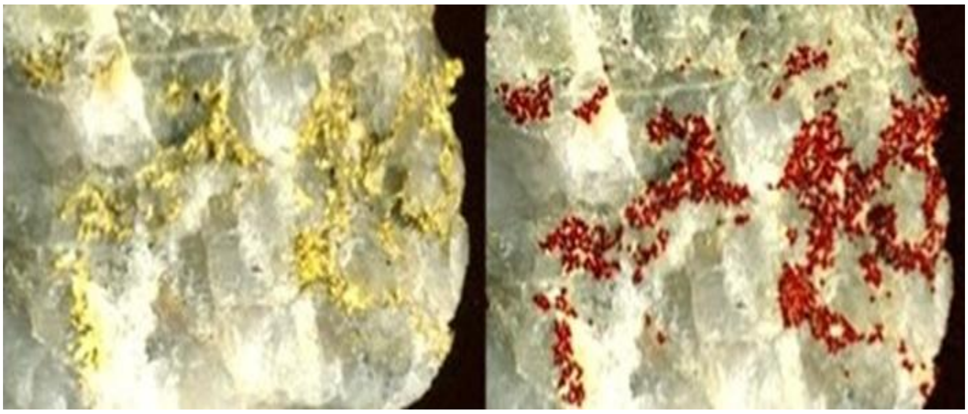

Figure 7: Zoomed-in view of the right part of Figures 5 and 6.

3.2. Determining Soil Elements

The colors in nature arise from various hues emitted by different elements sourced from rocks, soils, or vegetation. This facilitates the identification of elements in high-resolution images and permits the re-analysis of older images to retrieve information regarding their compounds and elements. Calcium is extracted from a natural calcium field and represented in yellow. The calcium element is identified and denoted with black dots via image processing (The MATLAB program, which was designed entirely for this research and included in the appendix, demonstrates the working mechanism for detecting calcium and gold elements. Any researcher can copy and use it to search for other elements at any location within colored maps captured from any satellite) some of which are illustrated in Figure 8(. The black dots in regions devoid of calcium signify the visual reflections of wavelengths emitted by the identical element.

Figure 8: The calcium element appears yellow in the left image [24], and after processing, it is represented by black dots.

Google Earth maps offer an extensive resource for this form of analysis. This study employed a map of Iraq to identify the locations of calcium elements. The research identified numerous locations with varying concentrations of calcium fields throughout Iraq, with a notable prevalence in the northwest and western regions, as depicted in Figure 9, which was captured from an altitude of 2,000 km using the Google Earth tool.

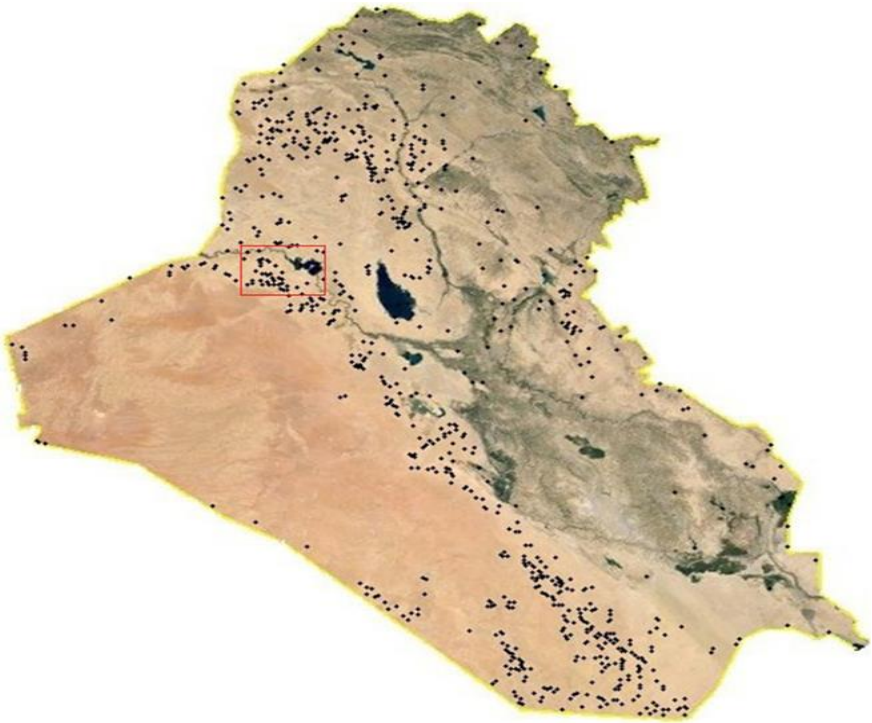

Figure 9: Calcium fields in northern Iraq identified through image processing, scale drawing 1.9/107.

Figure 9 indicates that Iraq's most significant and abundant calcium fields are located in Anbar province, west of Iraq, rather than in Mosul province, as indicated by the red square.

The map of calcium fields can be magnified to disclose further characteristics of the urban area being examined. Zooming in causes the image pixels to spread out, revealing new colors that indicate the presence of calcium fields. The red square in Figure 9, located at an altitude of 141 km, has an image width of 152 km (Figure 10).

Figure 10: New features of the calcium fields are identified, highlighted by black signs.

As zooming intensifies, numerous new landmarks become visible across diverse terrains. Upon examining the significant clusters, it is apparent that the land harbors a wide variety of minerals, suggesting the existence of diverse minerals, although they are frequently present in minimal quantities. These diminished concentrations cannot be considered viable fields for exploration. Consequently, it is imperative to rely on concentrations and substantial clusters, as these provide a more definitive representation of significant quantities in a specific region. The focus should be on the aggregation of cluster elements on the map rather than on discrete points (Figure 11). The width of the red square on the left side of Figure 12 is 20 km, and it is enlarged on the right side of the figure, positioned at an altitude of 44 km.

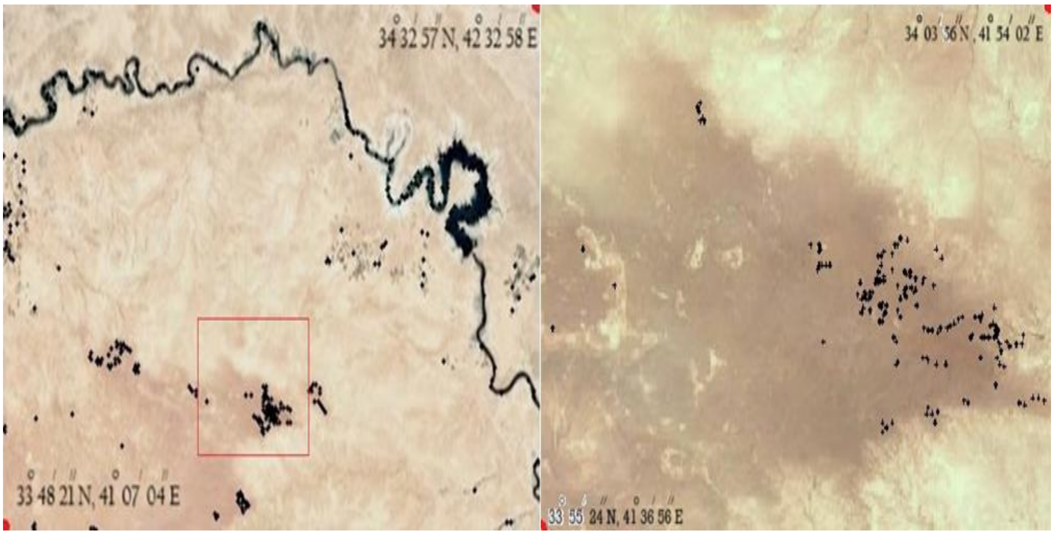

Figure 11: The red square (on the left side) indicates cluster concentrations of the calcium element, while the other white points scattered on the map do not necessarily represent actual fields.

The overlapping of pixel colors intensifies with each level of magnification. Thus, each pixel in the image exhibiting the same color and optical wavelength can be interpreted in three distinct ways. The Anbar region's vast territories are rich in this element, Figure 12. The red square on the left side of Figure 12, initially 8 km wide, was enlarged and is now positioned on the right side of the figure at an elevation of 11 km.

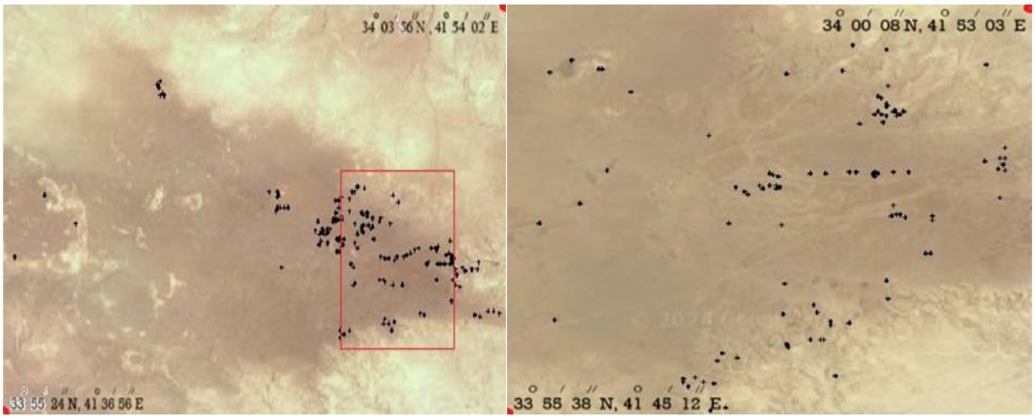

Figure 12: The black points indicate the presence of the calcium element in the Anbar west of Iraq.

Figure 12 illustrates a map of Iraq, marked by numerous black dots in the western and southwestern regions, signifying the presence of calcium in those locales. The widespread distribution of these dots indicates the presence of numerous calcium fields. Moreover, focusing on one of these regions uncovers novel distribution characteristics, as depicted in Figure 13. The red square illustrated on the left side of Figure 13 initially measures 2 km in width. Following enlargement, it is now situated on the right side of the figure at an altitude of 2 km.

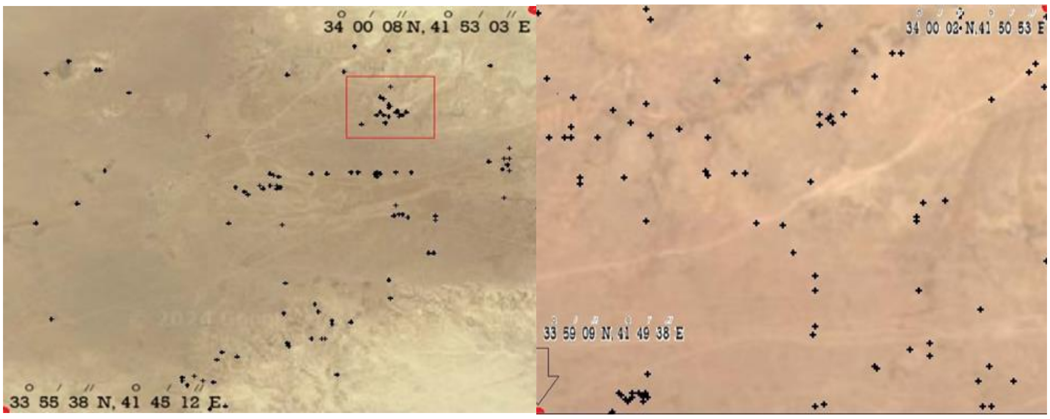

Figure 13: Calcium concentrations are measured at an altitude of 2 km (width of the red square) to appear on the right side.

The focal points relate to regions that draw interest or attention, which may change when the image is enlarged due to pixel separation and the appearance of new pixels exhibiting varying colors. As a result, the positions of these points may change as a pixel's previously blended color becomes more distinct when viewed at higher magnification. Increased magnification reveals further details, with pixels exhibiting subtle variations in color shades. Examining a specific section of Figure 13 results in the development of Figure 14. The red square on the left side of Figure 14 initially measured 200 m in width. Following enlargement, it was relocated to the right side of the figure, situated at an elevation of 700 m.

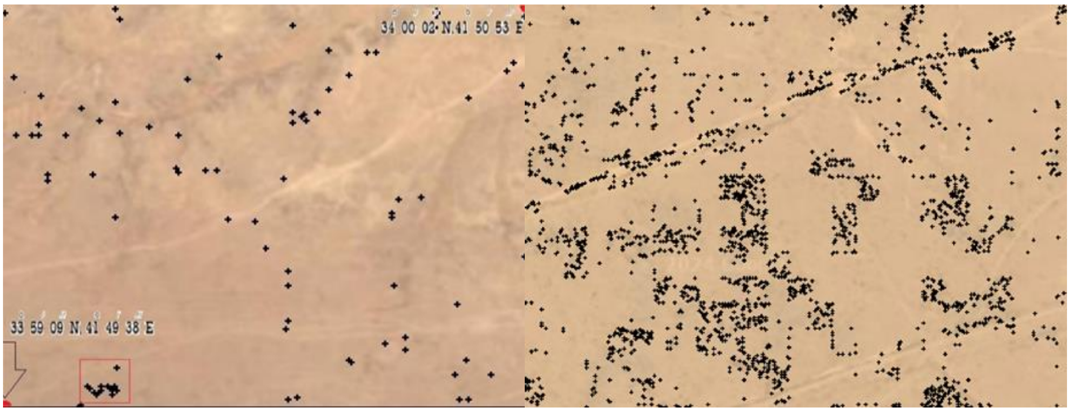

Figure 14: The result of one of the calcium (gypsum) deposits identified on the right side of the figure is only 200 m wide, and the image was taken from an altitude of 700 m.

The geographical boundaries of the right side of Figure 14 are as follows: upper right corner at 33° 59' 16" N, 41° 49' 53" E, and lower left corner at 33° 59' 06" N, 41° 49' 40" E. The image depicted on the right side of Figure 14 exhibits a width of 822 pixels across a distance of 200 m, indicating that each pixel corresponds to an approximate length of 24 cm.

This technique identifies locations of calcium (gypsum) accumulation, aiming to reduce field research costs and determine these locations accurately and efficiently. This approach enables companies to minimize both costs and time. This calcium field represents one of the numerous undiscovered fields in Iraq, and the site was selected randomly without prior specification. Gypsum is prevalent in Iraq, especially in the western and northwestern areas, including Anbar, Mosul, and Salah al-Din. The deposits extend southward to Karbala, Najaf, and the Al-Muthanna Governorate (Figure 9).

4. Conclusion

A research initiative focused on image processing methodologies to determine the average wavelength of monochromatic light without relying on traditional techniques such as prisms or diffraction gratings. By analyzing the density of focal points within a limited area, a distinct grouping was created to calculate the average wavelength from laser light sources. This approach eliminates the need for conventional optical instruments, providing a more efficient and accessible means for wavelength analysis. The results revealed errors in wavelength measurements, highlighting both the advantages and limitations of the methodology. The analysis revealed that substantial amounts of calcium deposits are predominantly located in the western and southwestern regions of Iraq, particularly in Al-Anbar Governorate, along the Euphrates River, and in areas adjacent to the Saudi border. The study also identified scattered fields in Mosul, Salah al-Din, and Diyala Governorate. The use of Google Earth and high-resolution images enabled the observation of alterations in the positions of these concentrations on maps. The study demonstrated the ability to accurately analyze elements based on map colors and pinpoint their locations on the ground by assessing their concentrations. The findings have practical implications for identifying and mapping mineral deposits, such as calcium deposits (gypsum), in Iraq.

5. Recommendations

This study focused on calcium elements, introducing a novel methodology that utilizes optical range techniques to examine soil components while also emphasizing the importance of validating the program's results. Future research should investigate additional elements on the Iraq map alongside continued studies of calcium deposits and mapping calcium fields. This information will enable companies to identify and operate in these areas with minimal effort swiftly.

References

[1] R. Chhabra and R. Chhabra, "Nature and origin of salts, classification, area and distribution of salt-affected soils," in *Salt-Affected Soils and Marginal Waters: Global Perspectives and Sustainable Management*, pp. 1–47, 2021. http://dx.doi.org/10.1007/978-3-030-78435-5_1.

[2] B. Towaranonte and Y. Gao, "Application of charge-coupled device (CCD) cameras in electrochemiluminescence: A minireview," *Anal. Lett.*, vol. 55, no. 2, pp. 186–202, 2022. https://doi.org/10.1080/00032719.2021.1920971.

[3] B. Rayegani, S. Barati, H. Goshtasb, S. Gachpaz, J. Ramezani, and H. Sarkheil, "Sand and dust storm sources identification: A remote sensing approach," *Ecological Indicators*, vol. 112, p. 106099, 2020. https://doi.org/10.1016/j.ecolind.2020.106099.

[4] M. Y. Kataev, E. Y. Kartashov, and I. B. Sorokin, "Determination of soil color characteristics using RGB images," *in Ecological Aspects of Soil and Land Preservation*. Hershey, PA, USA: IGI Global Scientific Publishing, 2024, pp. 225–251, https://doi.org/10.4018/979-8-3693-3374-7.ch009. .

[5] J. M. M. Linhares, J. A. R. Monteiro, A. Bailão, L. Cardeira, T. Kondo, S. Nakauchi, M. Picollo, C. Cucci, A. Casini, L. Stefani, and S. M. C. Nascimento, "How good are RGB cameras retrieving colors of natural scenes and paintings? A study based on hyperspectral imaging," *Sensors*, vol. 20, no. 21, p. 6242, 2020. https://doi.org/10.3390/s20216242.

[6] S. Zhang, Y. Yang, F. Sun, and B. Fang, "Application of image sensing system in mineral/rock identification: Sensing mode and information process," *Advanced Intelligent Systems*, vol. 5, no. 11, Art. no. 2300206, 2023. https://doi.org/10.1002/aisy.202300206.

[7] R. Cheng, Y. Zhou, S. Wang, M. Shen, T. Taher, and H. X. Tang, "A 100-pixel photon-number-resolving detector unveiling photon statistics," *Nature Photonics*, vol. 17, no. 1, pp. 112–119, 2023. https://doi.org/10.1038/s41566-022-01119-3.

[8] A. Deyasi, S. Mukherjee, P. Debnath, and A. K. Bhattacharjee, Eds., *Computational Science and Engineering: Proceedings of the International Conference on Computational Science and Engineering (Beliaghata, Kolkata, India, 4–6 October 2016*, 1st ed. CRC Press, 2016. https://doi.org/10.1201/9781315375021.

[9] V. Tyagi, *Content-based Image Retrieval: Ideas, Influences, and Current Trends*. Springer Singapore, 2018. https://doi.org/10.1007/978-981-10-6759-4.

[10] G. de Carvalho Oliveira, C. C. S. Machado, D. K. Inácio, J. F. da Silveira Petruci, and S. G. Silva, "RGB color sensor for colorimetric determinations: Evaluation and quantitative analysis of colored liquid samples," *Talanta*, vol. 241, p. 123244, 2022. https://doi.org/10.1016/j.talanta.2022.123244.

[11] P. McEvoy, *Capture and Simulation of Fluorescence in Fabrics: Estimating and Simulating Fluorescent Appearance in Fabrics Using LEDs and an RGB Camera*, 2020. https://hdl.handle.net/20.500.12380/302006.

[12] S. Covshoff, Ed., *Photosynthesis: Methods and Protocols*, pp. 1–300. Springer Nature, 2024. https://doi.org/10.1007/978-1-0716-3790-6

[13] F. Merchant and K. Castleman, Eds., Microscope Image Processing, 2nd ed. Elsevier, 2022. https://doi.org/10.1016/C2019-0-01813-4.

[14] J. R. Riba, "Application of image sensors to detect and locate electrical discharges: a review," *Sensors*, vol. 22, no. 15, p. 5886, 2022. https://doi.org/10.3390/s22155886.

[15] X. Xiaoqian, F. Fan, J. Siatong, W. Lu, A. Srivastava, and V. G. Chigrinov, "Evaluation of LC Fresnel phase plate utilized as colour filter," *Molecular Crystals and Liquid Crystals*, vol. 559, no. 1, pp. 228–240, 2012. http://dx.doi.org/10.1080/15421406.2012.661945.

[16] M. P. Edgar, G. M. Gibson, and M. J. Padgett, "Principles and prospects for single-pixel imaging," *Nature Photonics*, vol. 13, no. 1, pp. 13–20, 2019. https://doi.org/10.1038/s41566-018-0300-7.

[17] D. J. Kemp, M. E. Herberstein, L. J. Fleishman, J. A. Endler, A. T. Bennett, A. G. Dyer, *et al.*, "An integrative framework for the appraisal of coloration in nature," *The American Naturalist*, vol. 185, no. 6, pp. 705–724, 2015. https://doi.org/10.1086/681021.

[18] A. M. F. Al-Quraishi, B. M. Mustafa, P. Gopinathan, and Y. Divya, "Potential of multispectral satellite data for superficial iron oxide detection in Sulaimaniyah, Iraqi Kurdistan Region," *Journal*

of Applied Science and Technology Trends, vol. 3, no. 01, pp. 45–52, 2022. https://doi.org/10.38094/jastt301171.
[19] S. S. Abd Al-Qadir, A. K. Al-Ali, and B. H. Soltan, "Monitoring soil contamination by hydrocarbons and heavy metals in parts of Basra, Southern Iraq using remote sensing and GIS techniques," *The Iraqi Geological Journal*, vol. 56, no. 2E, pp. 29–42, 2023. https://doi.org/10.46717/igj.56.1d.3ms-2023-4-12.
[20] A. Al Maliki, U. S. Kumar, A. H. Falih, M. A. Sultan, A. Al-Naemi, D. Alshamsi, *et al*., "Geochemical processes, salinity sources and utility characterization of groundwater in a semi-arid region of Iraq through geostatistical and isotopic techniques," *Environmental Monitoring and Assessment*, vol. 196, no. 4, p. 365, 2024. http://dx.doi.org/10.1007/s10661-024-12533-1.
[21] Z. A. Aljubouri, "Geochemistry of calcium sulphate rocks of Fatha Formation at four localities within Nineveh District, Northern Iraq (with emphasis on strontium distribution)," *Iraqi National Journal of Earth Sciences*, vol. 11, no. 1, pp. 49–60, 2011. http://dx.doi.org/10.33899/earth.2011.5500.
[22] E. Instruments, "How to choose your lasers for Raman microscopy," *Edinburgh Instruments*, 2023. https://www.edinst.com/blog/lasers-for-raman-spectroscopy/.
[23] R. A. Viscarra Rossel, T. Behrens, E. Ben-Dor, D. J. Brown, J. A. M. Demattê, K. D. Shepherd, Z. Shi, B. Stenberg, A. Stevens, V. Adamchuk, H. Aïchi, B. G. Barthès, H. M. Bartholomeus, A. D. Bayer, M. Bernoux, K. Böttcher, L. Brodský, C. W. Du, A. Chappell, *et al*., "A global spectral library to characterize the world's soil," *Earth-Science Reviews*, vol. 155, pp. 198–230, 2016. https://doi.org/10.1016/j.earscirev.2016.01.012.
[24] Shutterstock, "Calcium carbonate mines," *Shutterstock*. https://www.shutterstock.com/search/calcium-carbonate-mines. [Accessed: Nov. 22, 2024].

Appendix

The MATLAB program (core work of this research) was used to determine the calcium and gold element

```
clc
clear all
close all
%This program for detrmination Calcium element
i=imread('Iraq4.jpg');
wavelength=577;
figure(1)
imshow(i)
[xx yy]=size(i(:,:,1));
r=0,g=0;b=0;r1=0;g1=0;b1=0;
n=0;p=i;t=0;Gold=0;Silver=0;u5=100;Nicle=0;u6=20;u7=10;
S=0;q=i;
% ______The spectral lines of calcium element has been taken from NIST site
Ca(1)=3706.026;Ca(2)=3736.901;Ca(3)=3933.6614;Ca(4)=3968.4673
;Ca(5)=4226.727;Ca(6)=4302.527;Ca(7)=4307.741;Ca(8)=4425.441;Ca(9)=4434.960;Ca(10)
=4435.688;Ca(11)=4454.781;Ca(12)=4455.887;
Ca(13)=4456.605;Ca(14)=4878.132;Ca(15)=5019.971;Ca(16)=5188.848;Ca(17)=5265.557;C
a(18)=5270.270
;Ca(19)=5349.472;Ca(20)=5581.971;Ca(21)=5588.757;Ca(22)=5590.120;Ca(23)=5594.468;C
a(24)=5598.487;
Ca(25)=5857.452;Ca(26)=6102.722;Ca(27)=6122.219;Ca(28)=6162.172;Ca(29)=6169.055;
Ca(30)=6169.559;Ca(31)=6439.073;Ca(32)=6449.810;Ca(33)=6456.874
;Ca(34)=6462.566;Ca(35)=6471.660;Ca(36)=6493.780;
Ca(37)=6499.649;Ca(38)=6572.777;Ca(39)=6717.685;Ca(49)=7148.147;
Ca(41)=7202.194;Ca(42)=7326.146;Ca(43)=7601.304;
```

```
Ca=Ca/10;
%______________________________________
% Au  Gold element
Au(1)=3557.365;  Au(2)=3586.731;Au(3)=3611.568;Au(4)= 3631.311;Au(5)= 3637.905;
Au(6)= 3645.016;Au(7)= 3650.739;Au(8)= 3709.622;Au(9)= 3796.007;Au(10)= 3897.865;
  Au(11)=   3909.383;Au(12)=     4040.931;   Au(13)=4065.068;Au(14)=   4315.110;Au(15)=
4437.269;
  Au(16)=      4488.253;Au(17)=      4607.512;Au(18)=      4792.583;      Au(19)=5230.259;
Au(20)=5837.374;
  Au(21)=5956.965;Au(22)= 6278.170;Au(23)=6562.680;Au(24)= 7510.728;
 Au=Au/10;
%  Number 10 is for converting to (nm) nano meter
 %_____________________________________________________
% converted parameter to G and j1 is the length of matrix

G=Ca;          % name of matrix
j1=43;         % number of matrix
Delta=5 ; % rate of error
%_________________________________________________
k=0;
e1=1;e2=1;e3=1;O=0;
h=0;
ii=i;
for loopred=650:10:720
   for loopblue=330:10:430
i=ii;
for y=2:1:yy;
   u2=0;
    for x=2:1:xx;
    n=n+1;
u= i(x,y,1);

u2=0;
for u1=1:1:u
   u2=u2+1;
end
Ir=u2;
Irr(n)=Ir;
u=i(x,y,2);
 u2=0;
for u1=1:1:u
   u2=u2+1;
end
Ig=u2;
Igg(n)=Ig;
u4=i(x,y,3);
 u2=0;
for u1=1:1:u4
   u2=u2+1;
end
```

```
 Ib=u2;
Ibb(n)=Ib;
%------------ CANCELED EFFECT OF WIGHT SPOT
if Ir>190

 end
%---------------
ITOTAL=Ir+Ig+Ib;
Ir=Ir*loopred;
Ig=Ig*550;
Ib=Ib*loopblue;
 I(x,y)=(Ir+Ig+Ib)/ITOTAL; % Each pixel has one wave length
 for j=1:1:j1

      if I(x,y)<G(j)+0.1;
          if I(x,y)>G(j)
          I(x,y);
if i(x,y,1)>0
    e1=0;

end
if i(x,y,2)>0
    e2=0;
end
if i(x,y,3)>0
    e3=0;

end
            i(x,y,1)=255*e1;
            i(x,y,2)=255*e2;
            i(x,y,3)=255*e3;
            %________________ recorder the data
            q(x,y,1)=i(x,y,1);
            q(x,y,2)=i(x,y,2);
            q(x,y,3)=i(x,y,3);

           % The surrounding pixels about base pixel
%            1_________________
             i(x+1,y,1)=255*e1;
              i(x+1,y,2)=255*e2;
           i(x+1,y,3)=255*e3;
%            2 ___________________
            i(x-1,y,1)=255*e1;
              i(x-1,y,2)=255*e2;
            i(x-1,y,3)=255*e3;
%            3 _____________________
            i(x,y+1,1)=255*e1;
            i(x,y+1,2)=255*e2;
           i(x,y+1,3)=255*e3;
 %           4 _____________________
```

```
          i(x,y-1,1)=255*e1;
            i(x,y-1,2)=255*e2;
        i(x,y-1,3)=255*e3;
S=S+1;
          end; end ; end; end ;end
S=S;
h=h+1;
hold on
    figure(1)
    imshow(i)
    pause(0.5)

   end
end
```